ACS Catalysis

Research Article

pubs.acs.org/acscatalysis

Role of Steric Attraction and Bite-Angle Flexibility in Metal-Mediated C−H Bond Activation

Lando P. Wolters,[†] Rick Koekkoek,[†] and F. Matthias Bickelhaupt*[,†,‡]

[†]Department of Theoretical Chemistry and Amsterdam Center for Multiscale Modeling, VU University, De Boelelaan 1083, NL-1081 HV Amsterdam, The Netherlands

[‡]Institute for Molecules and Materials, Radboud University Nijmegen, Heyendaalseweg 135, NL-6525 AJ Nijmegen, The Netherlands

Supporting Information

ABSTRACT: We show quantum chemically that, contrary to common believe, bulky ligands in d^{10}-ML_2 complexes may *enhance*, instead of counteract, L−M−L bite-angle bending. The resulting more flexible or even nonlinear geometry translates into lower barriers for oxidative addition of the methane C−H bond to these complexes. This follows from our quantum chemical analyses of the bonding in and reactivity of bisphosphine palladium complexes $Pd(PR_3)_2$ with varying steric bulk, based on relativistic dispersion-corrected DFT computations in combination with the activation strain model and quantitative MO theory. Ligands that are large but to some extent flat (instead of isotropically bulky) are shown to build up relatively strong dispersion interactions between their large surfaces ("sticky pancakes") when they bend toward each other. The resulting stabilization, a form of steric attraction, favors bending and thus enhances bite-angle flexibility. This leads to surprisingly low reaction barriers for methane C−H activation by the rather congested $Pd(PCy_3)_2$ and $Pd(PPh_3)_2$ model catalysts. Our findings not only explain the unexpected nonlinear L−M−L angles observed in crystallographic data but also more generally demonstrate the importance of dispersion interactions in realistic catalyst complexes. Perhaps most importantly, we reveal how the concept of steric attraction can serve as a tool for tuning bite-angle flexibility and thereby the activity of catalyst complexes.

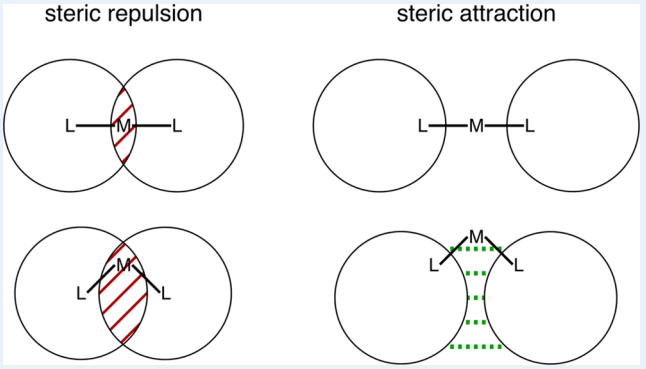

KEYWORDS: *activation strain model, bite angles, catalysis, density functional calculations, dispersion, oxidative addition, transition metal complexes*

INTRODUCTION

Palladium phosphine complexes are featured as catalysts in various versatile cross-coupling reactions, such as those developed by Heck, Stille, and Suzuki.[1] The first step in these cross couplings is the oxidative addition of a substrate to the transition metal complex (Scheme 1).

Scheme 1. Oxidative Addition and Reductive Elimination

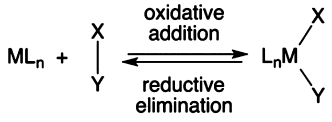

The bite angle, that is, the ligand−metal−ligand angle, is generally considered to be an important geometric parameter of a catalyst. It is known that a smaller bite angle leads to a lower barrier for the oxidative addition[2] because of less steric repulsion between the substrate and the ligands. In other catalytic processes (e.g., hydroformylation, hydrocyanation and Diels−Alder reactions), the bite angle is one of the parameters known to affect the activity as well as regioselectivity of the catalyst complex.[3] Control over the bite angle is usually achieved using bidentate ligands in which the coordinating sites are bridged by, for example, a hydrocarbon chain of variable length. A study on palladium complexes with chelating ligands addressed the precise nature of the bite-angle effect on oxidative addition reaction barriers.[4] The results clearly indicate that a catalyst with a smaller bite angle displays higher reactivity because it does not have to bend away its ligands to avoid repulsive interactions of the ligands with the substrate. Thus, the bite angle effect on reaction barriers is primarily steric in nature. The electronic nature,[5] that is, stabilization of the transition state due to stronger donor−acceptor orbital interactions from metal d orbitals to the substrate σ^* orbital as the metal−ligand d-hybrid orbital is pushed up in energy at smaller bite angles, has a much smaller effect on the reaction barrier.

Received: June 27, 2015
Revised: August 19, 2015
Published: September 1, 2015

DOI: 10.1021/acscatal.5b01354
ACS Catal. 2015, 5, 5766−5775

The active catalytic species in cross-coupling reactions, however, is often a dicoordinated d^{10}-ML_2 complex, where L is a nonchelating ligand. Geometries of d^{10}-ML_2 transition metal complexes are generally assumed to have linear ligand−metal−ligand angles.[2c,6−9] In a recent study on small d^{10}-ML_2 complexes (M = Co^-, Rh^-, Ir^-, Ni, Pd, Pt, Cu^+, Ag^+, or Au^+; L = NH_3, PH_3, or CO), we found significantly bent complexes, with ligand−metal−ligand angles up to 128.6° for $Co(CO)_2^-$.[10] More importantly, we explained the origin of their nonlinearity. Our analyses revealed that a number of d^{10}-ML_2 complexes prefer nonlinear geometries because the two ligands then do not compete for π backdonation from the same d orbital. Of course, to prefer a nonlinear geometry, the additional stabilization that results from this effect must be greater than the additional steric repulsion that occurs upon bending. In a study on the reactivity of these complexes toward methane addition,[11] we found that even along series of linear complexes, these electronic effects influence the height of the reaction barrier because they lead to differences in flexibility of the ligand−metal−ligand angles. This result indicates that a structural parameter based on the equilibrium geometry, such as the bite angle, is not necessarily sufficient to predict the catalyst's activity. Better insights can be obtained when not the bite angle itself, but the bite-angle flexibility is considered.

A different study on halogen-substituted $Pd(PX_3)_2$ complexes (X = F, Cl, Br, or I) confirmed these insights and furthermore showed that attractive dispersion interactions between the ligands can lead to even smaller L−M−L angles in the PdL_2 complexes with heavier halogens on the phosphines.[12] We found that all halogenated $Pd(PX_3)_2$ complexes are intrinsically bent, whereas $Pd(PH_3)_2$ is linear. Along $Pd(PF_3)_2$, $Pd(PCl_3)_2$, $Pd(PBr_3)_2$, and $Pd(PI_3)_2$, the P−Pd−P angle decreases from 151.7° to 122.4° as a result of a decreased occupied−occupied orbital overlap upon bending the catalyst, further accompanied by attractive dispersion interactions that become stronger when the halogens become heavier along F, Cl, Br, and I. Also for these complexes, direct ligand−ligand repulsion plays no dominant role.

Most phosphine-ligated catalysts used in practical applications of cross couplings, however, feature hydrocarbon substituents that are much bulkier than the hydrogens or halogens in these model catalysts. Many studies have addressed the steric properties of such ligands[13] and their effect on reactivity.[14] One might expect that the propensity to bend is decreased because the more bulky ligands will tend to avoid mutual steric repulsions. $Pd(PtBu_3)_2$ (*t*Bu = *tert*-butyl) is indeed known to have a 180° ligand−metal−ligand angle.[15] However, a crystal structure of $Pd(PPh(tBu)_2)_2$ (Ph = phenyl) obtained by Otsuka et al.[16] reveals a bite angle of 177.0°, and Immirzi and Musco reported a crystal structure of $Pd(PCy_3)_2$ (Cy = cyclohexyl) showing a bite angle of only 158.4°.[17] In addition, the analogous platinum complex $Pt(PCy_3)_2$ appears to have a nonlinear L−M−L angle of 160.5°, as revealed by crystallographic data.[18] Leitner et al. have reported[19] computational results on the structures of dicoordinated palladium phosphine compounds and found nonlinear P−Pd−P angles for a number of complexes. Notably, for $Pd(PCy_3)_2$, they obtained an angle of 162°, in reasonable agreement with the crystal structure. Many other computational studies, however, reported linear geometries or deviations from linearity of only a few degrees.[20−25]

Despite the available experimental data, and numerous computational studies on palladium phosphine complexes, to the best of our knowledge, the observed nonlinearity has never been explained. In this work, we discuss a series of dicoordinated palladium complexes $Pd(PR_3)_2$ with phosphine ligands PR_3 of varying steric bulk in which R = hydrogen (H), methyl (Me), isopropyl (*i*Pr), *tert*-butyl (*t*Bu), cyclohexyl (Cy), or phenyl (Ph). Interestingly, although the expected linear geometries emerge for $Pd(PH_3)_2$, $Pd(PMe_3)_2$, and $Pd(PtBu_3)_2$, we find that $Pd(PiPr_3)_2$, $Pd(PCy_3)_2$, and $Pd(PPh_3)_2$ have increasingly nonlinear bite angles of 172.4°, 148.2°, and even 132.2°, respectively. We relate these findings to the precise steric properties of the ligands, that is, size but also shape. Activation strain analyses in combination with quantitative MO theory explain this dichotomy because they reveal that steric bulk may operate in two distinct ways: (i) one mechanism is the usual steric repulsion deriving from overlap between closed-shell orbitals of intimate and isotropically bulky ligands; (ii) the second mechanism embodies steric attraction,[26] which occurs as a result of dispersion interactions between anisotropically bulky ligands (e.g., flat ligands with a large surface) that are not yet in direct contact. Although the importance of dispersion interactions has been noted by several research groups in the past,[25,27−31] it is often believed that its energetic effect is moderate and arises only because of additional intermolecular attraction. Here, we show that intramolecular dispersion interactions can also be of paramount importance to obtain both qualitatively and quantitatively correct results. Furthermore, we reveal how steric attraction results in improved bite-angle flexibility of the catalyst complexes. This leads to surprisingly low reaction barriers for methane C−H activation, even for rather congested model catalysts, such as $Pd(PCy_3)_2$ and $Pd(PPh_3)_2$.

THEORETICAL METHODS

Computational Details. All calculations were carried out using the Amsterdam Density Functional (ADF) program developed by Baerends and co-workers[32−34] and the Quantum-regions Interconnected by Local Descriptions (QUILD) program.[35] The numerical integration was performed using the procedure developed by te Velde et al.[36] For the flat potential energy surface for bending $Pd(PPh_3)_2$, we used the Becke integration scheme that has become available with the ADF2013 release.[37] The MOs were expanded in a large uncontracted set of Slater type orbitals (STOs): TZ2P (no Gaussian functions are involved). The TZ2P basis set[38] is of triple-ζ quality for all atoms and has been augmented with two sets of polarization functions, that is, 2p and 3d on H, 3d and 4f on C and P, and 5p and 4f on Pd. An auxiliary set of s, p, d, f and g STOs was used to fit the molecular density and to represent the Coulomb and exchange potentials accurately in each self-consistent field (SCF) cycle. All electrons are included in the variational treatment (no frozen-core approximation used).

Equilibrium structures were obtained by optimizations using analytical gradient techniques.[39] Geometries and energies were calculated at the BLYP level of the generalized gradient approximation (GGA): exchange is described by Slater's $X\alpha$ potential,[40] with nonlocal corrections due to Becke[41] added self-consistently, and correlation is treated using the gradient-corrected functional of Lee, Yang and Parr,[42] with dispersion corrections using Grimme's third-generation DFT-D3 method.[43] In this approach, the density functional is augmented with an empirical term correcting for long-range dispersion effects, described by a sum of damped interatomic potentials of the

DOI: 10.1021/acscatal.5b01354
ACS Catal. 2015, 5, 5766−5775

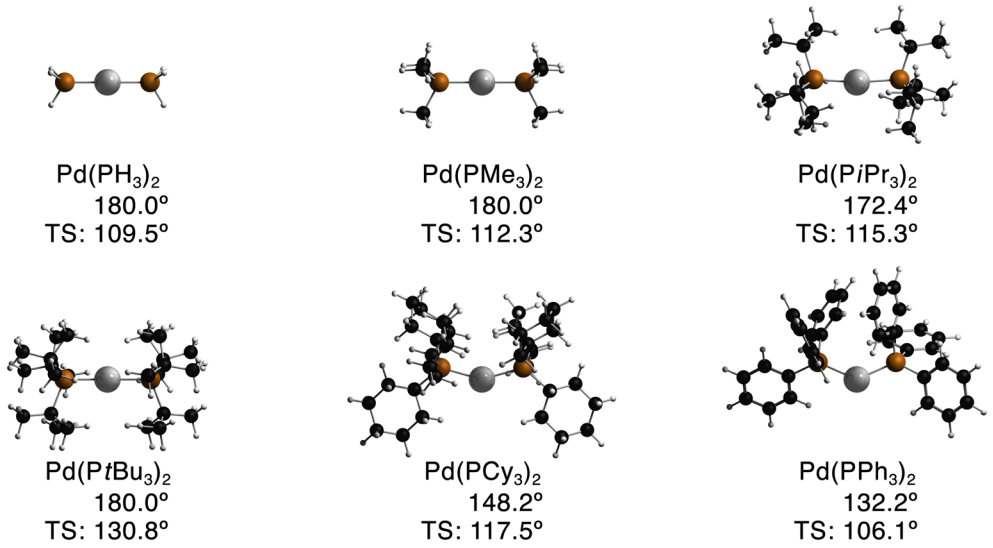

Figure 1. Equilibrium geometries and P−Pd−P angles (TS: value in TS for methane C−H activation) of palladium−phosphine complexes, computed at ZORA−BLYP−D3/TZ2P.

form C_6R^{-6} added to the usual DFT energy. Scalar relativistic effects were accounted for using the zeroth-order regular approximation (ZORA).[44]

Solvent effects in toluene have been estimated by applying the conductor-like screening model (COSMO)[45] as implemented in the ADF program[46] to the gas-phase geometries. A dielectric constant of 2.38 and a solvent radius of 3.48 Å are used for toluene, and atomic radii are taken from the MM3 van der Waals radii,[47] scaled by 0.8333.[48] Work by Riley et al. suggests that the dispersion correction does not need to be modified when combined with implicit solvation models.[49]

Energy minima and transition states have been verified through vibrational analysis.[50] All minima were found to have zero imaginary frequencies, whereas transition states have one. The potential energy surface (PES) around the transition state of the oxidative addition reactions has been approximated using the transition-vector approximation to the IRC (TV-IRC) method[51] to avoid the significant computational cost of full intrinsic reaction coordinate (IRC) calculations.[52,53] The PyFrag program was used to facilitate the analyses of the PESes.[54] Atomic charge analyses are performed using the Voronoi deformation density (VDD) scheme.[55]

Activation Strain Analyses. The bonding energy, ΔE, between two fragments is analyzed using the activation strain model.[56] Within this model, the potential energy surface $\Delta E(\zeta)$ is decomposed along the reaction coordinate ζ (or just at one point—for example, at the transition state, where $\Delta E(\zeta_{TS}) = \Delta E^{\ddagger}$—to obtain insight into the barrier height) into the strain energy, $\Delta E_{strain}(\zeta)$, that is associated with the geometrical deformation of the individual reactants as the process takes place, plus the actual interaction energy, $\Delta E_{int}(\zeta)$, between the deformed reactants (eq 1).

$$\Delta E(\zeta) = \Delta E_{strain}(\zeta) + \Delta E_{int}(\zeta) = \Delta E_{strain}(cat)(\zeta) + \Delta E_{strain}(sub)(\zeta) + \Delta E_{int}(\zeta) \quad (1)$$

To obtain insightful results, it is important to choose a proper reaction coordinate. For oxidative additions, the elongation of the bond that is broken has been shown to be a suitable parameter onto which to project the reaction coordinate.[51] The activation strain analyses in the present work are therefore projected onto the stretch of the activated bond. The strain energy can be divided into contributions $\Delta E_{strain}(cat)$ from the catalyst and $\Delta E_{strain}(sub)$ from the substrate (eq 1).

Molecular Orbital and Energy Decomposition Analyses. The interaction energy, $\Delta E_{int}(\zeta)$, between two molecular fragments is analyzed in the conceptual framework provided by the Kohn−Sham molecular orbital method. To this end, it is decomposed into three physically meaningful terms (eq 2) using a quantitative energy decomposition scheme.[57] This scheme is augmented with a fourth term, $\Delta E_{disp}(\zeta)$, which comprises the contributions from the dispersion interaction between the fragments.

$$\Delta E_{int}(\zeta) = \Delta V_{elstat}(\zeta) + \Delta E_{Pauli}(\zeta) + \Delta E_{oi}(\zeta) + \Delta E_{disp}(\zeta) \quad (2)$$

The term ΔV_{elstat} corresponds to the classical Coulomb interaction between the unperturbed charge distributions of the deformed reactants and is usually attractive. The Pauli repulsion energy, ΔE_{Pauli}, comprises the destabilizing interactions between occupied orbitals on the fragments and is responsible for steric repulsion. The orbital interaction energy, ΔE_{oi}, accounts for charge transfer (interaction between occupied orbitals on one fragment with unoccupied orbitals on the other fragment, including the HOMO−LUMO interactions) and polarization (empty-occupied orbital mixing on one fragment as a result of the presence of another fragment).

RESULTS AND DISCUSSION

Geometries of Catalyst Complexes. Figure 1 shows the equilibrium geometries for the series of $Pd(PR_3)_2$ complexes, following from our DFT computations at the dispersion-corrected ZORA−BLYP−D3/TZ2P level of theory. We find linear bite angles for $Pd(PH_3)_2$, $Pd(PMe_3)_2$, and $Pd(PtBu_3)_2$, whereas $Pd(PiPr_3)_2$, $Pd(PCy_3)_2$, and $Pd(PPh_3)_2$ have bent equilibrium geometries. $Pd(PiPr_3)_2$ is bent slightly, having a bite angle of 172.4° and being less than 0.1 kcal mol^{-1} more stable than the linear geometry. For $Pd(PCy_3)_2$, we find an angle of 148.2°, in rather good agreement with the available X-

DOI: 10.1021/acscatal.5b01354
ACS Catal. 2015, 5, 5766−5775

Table 1. M−L Bond Analysis[a] for the Monocoordinated PdL Complexes, Relative to the Ground State ($d^{10}s^0$) Pd Atom and the Ligand[b]

	M−L	VDD Pd	ΔE	ΔE_{int}	ΔV_{elstat}	ΔE_{Pauli}	ΔE_{oi}	ΔE_{disp}
$PdPH_3$	2.174	−0.044	−40.9	−41.2	−165.6	+189.4	−63.6	−1.4
$PdPMe_3$	2.186	−0.125	−49.0	−49.5	−189.9	+208.0	−63.6	−4.0
$PdPiPr_3$	2.210	−0.064	−52.8	−53.4	−185.8	+202.1	−61.9	−7.8
$PdPtBu_3$	2.228	−0.042	−53.1	−53.7	−181.6	+198.2	−61.1	−9.2
$PdPCy_3$	2.209	−0.009	−53.5	−54.1	−187.0	+203.1	−61.8	−8.4
$PdPPh_3$	2.198	−0.055	−49.7	−50.0	−175.0	+195.1	−63.2	−7.0

[a]In Å, electrons, kcal mol^{-1}. [b]Computed at ZORA−BLYP−D3/TZ2P.

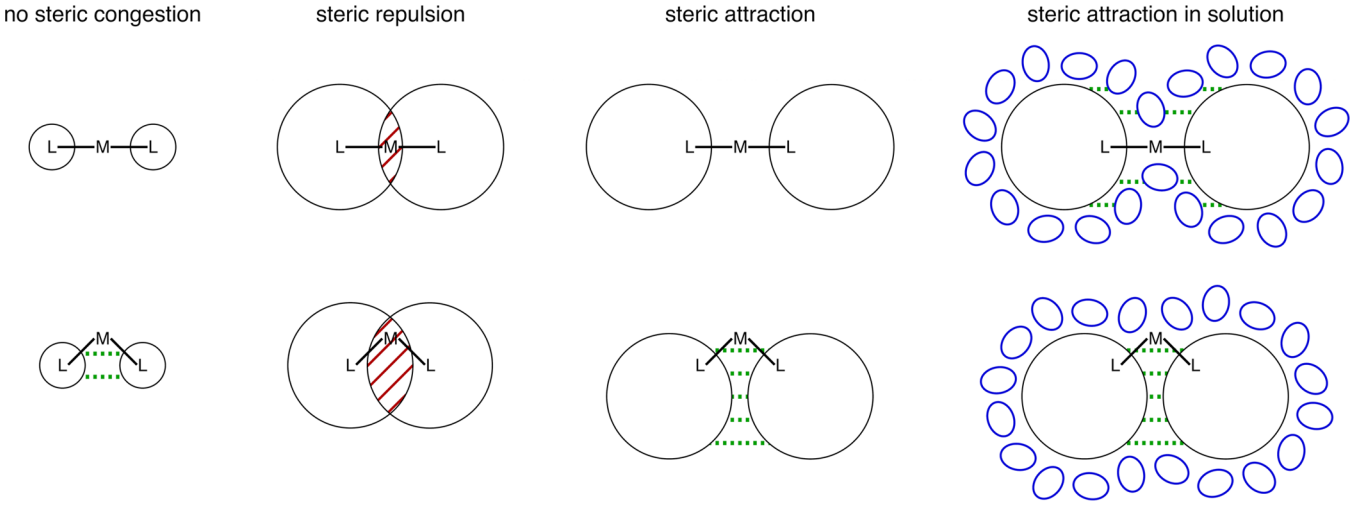

Figure 2. Schematic representation of different steric situations in ML_2 complexes. For the situation in solution, only the relevant interactions that occur in the region between the ligands are indicated.

ray structure.[17] $Pd(PPh_3)_2$ is even more bent, having a ligand−metal−ligand angle of only 132.2°. These latter angles are surprisingly small, given that the much less bulky $Pd(PH_3)_2$, for which one would expect even less resistance toward bending, is linear. We will show, however, that the greater steric dimension in $Pd(PCy_3)_2$ and $Pd(PPh_3)_2$ is, counterintuitively, of key importance to rationalize their nonlinearity.

In previous studies,[10,12] we have shown that most dicoordinated transition metal complexes have very flat potential energy surfaces for decreasing the ligand−metal−ligand angle to values smaller than 180°, due to enhanced π backbonding when the ligands interact with different d orbitals on the metal center. This additional stabilizing interaction can in some cases (i.e., for strong π-accepting ligands at an electron-donating metal center) outweigh the increased steric repulsion that occurs for smaller ligand−metal−ligand angles, leading to nonlinear ML_2 complexes.[10] To see if the same explanation holds for the $Pd(PR_3)_2$ complexes studied here, we have performed brief Pd−PR_3 bond analyses. The results (shown in Table 1) for the monocoordinated $PdPR_3$ complexes (R = H, Me, *i*Pr, *t*Bu, Cy, Ph) show that, in the present series, the trend in nonlinearity appears not to be caused by the π-backbonding capabilities. This is indicated by the small variation in the orbital interaction term (which for all complexes is between −61.1 and −63.6 kcal mol^{-1}), and the VDD charge on the palladium center changes irregularly instead of systematically. In the previous study, we found much larger and more systematic variations of these terms. Furthermore, the populations of the π-donating orbitals on Pd (i.e., the d_{xz} and d_{yz} orbitals when the Pd−PR_3 bond is aligned with the *z* axis) are essentially equal for each complex and consistently between 1.88 and 1.90 electrons.

These results therefore indicate that, although π backbonding contributes to the bite-angle flexibility of each of these complexes, it is not the dominant factor leading to their bent equilibrium geometries. This is confirmed by geometry optimizations of the $Pd(PR_3)_2$ complexes at the dispersion-free, but otherwise similar ZORA-BLYP/TZ2P level of density functional theory, at which we find the angles of the bent complexes to be increased to 173.9° for $Pd(PiPr_3)_2$, 179.4° for $Pd(PCy_3)_2$, and 180.0° for $Pd(PPh_3)_2$. Thus, although the slightly bent ligand−metal−ligand angle for $Pd(PiPr_3)_2$ is indicative for stronger π backbonding, or weaker repulsion, in this complex, the bent geometries of $Pd(PCy_3)_2$ and $Pd(PPh_3)_2$ originate from dispersive ligand−ligand attraction. In the following, we will therefore elaborate on the steric characteristics of the ligands and show that sterically repulsive bulk should be distinguished from sterically attractive bulk. The latter is of crucial importance to explain the observed ordering of the ligand−metal−ligand angles along the $Pd(PR_3)_2$ series in the present study.

To explain the different ways in which steric bulk can operate, we distinguish three situations that can occur for ML_2 complexes, schematically displayed in Figure 2. First, when small, nonbulky ligands are present, there is no significant steric congestion, and the complex is relatively indifferent toward bending its ligand−metal−ligand angle. For these complexes, the electronic effects, as mentioned before and described in ref 10, are decisive. Second, for the larger, bulkier ligands, steric effects are obviously more important. These effects are

DOI: 10.1021/acscatal.5b01354
ACS Catal. 2015, 5, 5766−5775

generally considered to be unfavorable for bending. In a sterically crowded situation, displayed schematically in the center of Figure 2, there is already in the linear geometry some ligand−ligand repulsion. Bending the ligands toward each other strengthens this steric repulsion by increasing the number of closed-shell/closed-shell (Pauli, or steric) repulsions. Third, however, as we have just seen, steric effects can also be favorable for bending. When the ligands are sizable, but not as sterically crowded, as displayed on the right of Figure 2, there is less steric congestion, and bending barely induces repulsion between the ligands. Instead, decreasing the L−M−L angle brings the ligands closer to each other and strengthens attractive dispersion interactions between the contact surfaces of the ligands. This "sticky-pancake" effect stabilizes a nonlinear geometry and becomes stronger as the shape of ligands becomes more flat, leading to larger contact surfaces.

In solution, this picture still applies. The presence of a solvent does not alter the situation for small ligands or for ligands with isotropically bulky substituents because there are no significant dispersion interactions to be quenched, and any repulsive interaction still persists. The effect of solvents on steric attraction, however, is moderate, as well. In the linear situation, the solvent molecules can occupy the space between the ligands, giving rise to some dispersion interactions between the ligand and the solvent (see Figure 2, the very right). When the ligands are bent toward each other, these solvent molecules are pushed out from between the ligands, leading again to a situation similar to that of the gas phase, but now within a solvent shell. This may go with some quenching of the net ligand−ligand dispersion stabilization upon bending when the ligand−solvent interaction becomes of comparable magnitude as the ligand−ligand interaction by which it is replaced in the bent configuration. The important point, however, is that the PES for L−M−L bending remains shallow. In other words, the L−M−L bite angle of complexes with bulky yet flat ligands remains flexible in solution, making it still easy to adopt a bent geometry.

Thus, especially for the small L−M−L angles encountered in chemical reactions of these complexes (as we will discuss in a later section), solvent effects can be expected to play no significant role, and the most important characteristics can be recovered from analyses in vacuo, which we therefore choose to discuss in the following sections.

These schematic representations allow us to rationalize the trend encountered along the series of $Pd(PR_3)_2$ complexes. To do so, it is important to consider the bite-angle flexibility of the catalyst complexes instead of only the value of the ligand−metal−ligand angle in the equilibrium geometry. To investigate the flexibility of the bite angle, we have computed the energy profiles for bending the L−M−L angle of the complexes from 180° toward 90° while all other geometry parameters are allowed to relax (see Figure 3). We find for all complexes, a rather flat energy profile between 180° and 150°, indicative for additional π backbonding upon bending, which compensates for (part of) the steric repulsion. Thereafter, the curves start to ascend as a result of dominating repulsive effects. The increase is least steep for $Pd(PH_3)_2$, which has the smallest substituents and is an example of a catalyst complex that is sterically indifferent toward bending. Going from $Pd(PH_3)_2$ to $Pd(PMe_3)_2$, $Pd(PiPr_3)_2$, and $Pd(PtBu_3)_2$, the steric bulk on the ligands is gradually increased and, thereby, also the bite-angle rigidity. This is indicated by the more steeply increasing energy profiles in Figure 3, and correlates well with the larger Tolman's

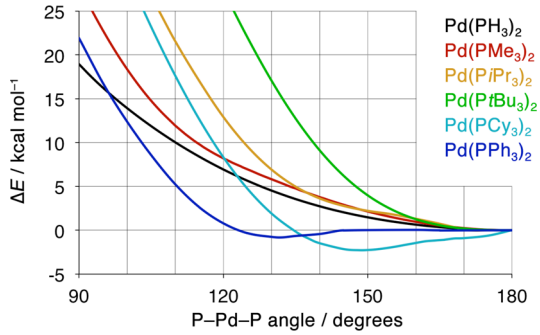

Figure 3. Potential energy surfaces for bending $Pd(PR_3)_2$ complexes, computed at ZORA−BLYP−D3/TZ2P.

cone angles along this series of ligands, which are 87°, 118°, 160°, and 182°, respectively.[58] Other parameters, such as the solid cone angles, reveal a similar trend for the series of ligands in this work.[59,60] Note that $Pd(PiPr_3)_2$ is bent slightly also when dispersion is neglected, but the bent equilibrium geometry is only marginally more stable than the linear geometry. We therefore conclude that its bending is the result of a delicate balance between the enhanced π backbonding and the opposing steric repulsion. On a flat potential energy surface, the position of the minimum is sensitive even to minor variations in the energy components.

Going from $Pd(PtBu_3)_2$ to $Pd(PCy_3)_2$ and $Pd(PPh_3)_2$, the ligands remain quite sizable, but the bulk is less isotropically distributed. The cyclohexyl substituents are not as bulky as *tert*-butyl substituents because they do not bind to the phosphorus atom via a tertiary carbon atom and rotate to avoid steric repulsion when the ligands are bent toward each other. In addition, there is room between the ligands, allowing the cyclohexyl substituents to rotate such that the attractive dispersion interactions between the ligands are enhanced. Going to the phenyl substituents reduces the bulkiness even further because these cyclic substituents consist of planar sp^2-hybridized carbon atoms instead of tetrahedral sp^3-hybridized carbon atoms. This leads to even less steric crowding between the ligands and, therefore, stronger steric attraction and consequently a smaller value of the bite angle. Again, this is in agreement with Tolman's cone angles, which for PCy_3 (170°) and PPh_3 (145°) are smaller than for $PtBu_3$ (182°).[58] The effect of steric attraction manifests itself also clearly when the bite-angle flexibility is considered: in addition to first descending to a minimum upon reducing the L−M−L angle from 180°, the bending energy profiles for these complexes are in general not very destabilized at smaller angles. The bending energy profile for $Pd(PCy_3)_2$ remains below that of $Pd(PiPr_3)_2$, even for angles as small as 100°, whereas that of $Pd(PPh_3)_2$ remains below even that of $Pd(PH_3)_2$ in this range.

Note that a similar reasoning can be used to account for the recent finding by Zhang and Dolg that the sterically more crowded syn isomer of a double C_{60} adduct of pentacene is more stable than the anti one.[61] In addition, such sterically attracting substituents can be considered to act as dispersion energy donors, a term recently introduced by Grimme and Schreiner.[62]

The potential energy surfaces in Figure 3 contain only the geometries connected to the energetically lowest conformations found. For all but the smallest complexes (i.e., all but $Pd(PH_3)_2$ and $Pd(PMe_3)_2$), we found other local minima at higher energies, in which one or more of the substituents have been

DOI: 10.1021/acscatal.5b01354
ACS Catal. 2015, 5, 5766−5775

Table 2. Geometries[a] and Activation Strain Analyses[b] for the Transition States of the Oxidative Addition of Methane[c]

	L−M−L[d]	C−H	$\Delta E^{\ddagger}$[e]	$\Delta E^{\ddagger}_{strain}$	$\Delta E^{\ddagger}_{strain}$(cat)	$\Delta E^{\ddagger}_{strain}$(sub)	$\Delta E^{\ddagger}_{int}$
$Pd(PH_3)_2$	109.5 (180.0)	1.734	+29.5 [+29.9]	+80.1	+16.4	+63.8	−50.7
$Pd(PMe_3)_2$	112.3 (180.0)	1.641	+28.4 [+28.8]	+72.3	+17.9	+54.4	−43.9
$Pd(PiPr_3)_2$	115.3 (172.4)	1.712	+30.0 [+29.7]	+79.6	+16.2	+63.4	−49.6
$Pd(PtBu_3)_2$	130.8 (180.0)	1.962	+43.1 [+42.7]	+108.9	+22.4	+86.6	−65.8
$Pd(PCy_3)_2$	117.5 (148.2)	1.729	+31.1 [+31.1]	+81.5	+17.9	+63.6	−50.3
$Pd(PPh_3)_2$	106.1 (132.2)	1.700	+20.9 [+20.8]	+71.0	+10.7	+60.3	−50.0

[a]Degrees, Å. [b]kcal mol^{-1}. [c]Computed at ZORA−BLYP−D3/TZ2P. [d]In parentheses, the value of the ligand−metal−ligand angle in the isolated catalyst complex. [e]Values in square brackets include solvation effects, computed for toluene with the COSMO model.

Table 3. Geometries[a] and Activation Strain Analyses[b] for the Product Complexes of the Oxidative Addition of Methane.[c]

	L−M−L[d]	C−H	ΔE[e]	ΔE_{strain}	ΔE_{strain}(cat)	ΔE_{strain}(sub)	ΔE_{int}
$Pd(PH_3)_2$	107.2 (180.0)	2.430	+24.3 [+23.2]	+134.5	+18.6	+115.8	−110.2
$Pd(PMe_3)_2$	107.6 (180.0)	2.512	+19.0 [+17.9]	+141.0	+21.9	+122.0	−122.0
$Pd(PiPr_3)_2$	111.8 (172.4)	2.341	+25.8 [+24.6]	+133.9	+20.5	+113.4	−78.8
$Pd(PtBu_3)_2$	129.7 (180.0)	2.112	+43.1 [+42.6]	+122.0	+24.0	+97.9	−78.8
$Pd(PCy_3)_2$	112.2 (148.2)	2.402	+26.3 [+25.4]	+139.8	+24.4	+115.4	−113.5
$Pd(PPh_3)_2$	102.6 (132.2)	2.417	+15.4 [+14.7]	+126.9	+14.0	+112.9	−111.4

[a]Degrees, Å. [b]kcal mol^{-1}. [c]Computed at ZORA−BLYP−D3/TZ2P. [d]In parentheses, the value of the ligand−metal−ligand angle in the isolated catalyst complex. [e]Values in square brackets include solvation effects, computed for toluene with the COSMO model.

rotated (see Table S2 of the Supporting Information). Most notably, for $Pd(PiPr_3)_2$, we also encountered a linear L−M−L structure at 8.2 kcal mol^{-1} above the global minimum with its angle of 172.4°, and for $Pd(PCy_3)_2$, a slightly *more* bent (146.8°) conformer was found at 2.7 kcal mol^{-1} as well as a less bent geometry (158.3°) at 0.5 kcal mol^{-1} above the global minimum, which assumes a bite angle of 148.2° (see Table 2). This latter angle matches the value of 158.4° from the crystal structure[17] better than the angle of 148.2° in the global minimum. Note, however, that the same is not true for the more rigid geometry parameters, such as the Pd−P bond lengths and the orientation of the substituents, for which significantly better agreement is achieved between our global minimum and the crystal structure.

For $Pd(PPh_3)_2$, the global minimum appears to be further stabilized by three C−H···π interactions occurring in a "Z" pattern between the phenyl rings on the different ligands (see Figure 1). A different local minimum is obtained when the ligands are in nearly eclipsed positions and the phenyl rings on one ligand are oriented perpendicular to each other as well as to the phenyl rings on the other ligand. This leads to only two possible C−H···π interactions between the ligands and a corresponding geometry with a larger bite angle of 141.0° and a 0.7 kcal mol^{-1} higher energy. We have not further analyzed the exact nature of these interactions[63] because this is beyond the scope of the present work and, as we noted before, the geometry assumes a linear bite angle if dispersion is not accounted for. This suggests that any eventual contribution from the C−H···π interactions to the stability of the nonlinear geometry is not as important as that from the dispersion interactions. In addition, when the complex is bent to smaller angles, as during the oxidative addition to which we will soon turn our focus, the phenyl rings more closely adopt a face-to-face orientation, further reducing the likelihood of any significant stabilizing contribution from C−H···π interactions.

Effect of Steric Attraction on Reaction Profiles for Oxidative Addition. In this second part, we explore the consequences of steric attraction and the resulting catalyst bite-angle flexibility or nonlinearity on the energy profiles of methane oxidative addition reactions. For both oxidative addition and its reverse reaction, reductive elimination, it is well-known that the bite angle of the catalyst complex has a great influence on the activity and selectivity of the process.[2,3] Recently, we introduced the concept of bite-angle flexibility as an improved descriptor of this parameter because it emerged from a study on small model catalysts.[11] We here test if our previous findings remain relevant when the realistic catalyst complexes in the present study are applied. To this end, we have studied the addition of the methane C−H bond to the palladium center of the series of $Pd(PR_3)_2$ complexes (with R = H, Me, *i*Pr, *t*Bu, Cy, and Ph) analyzed above. We chose the archetypal methane C−H bond as a simpler but representative model for the aryl halide bonds used more commonly in practice. From previous work,[4,11] it is known that catalyst−substrate prereaction complexes essentially do not exist for dicoordinated catalysts or are held together only by weak dispersion interactions. We therefore have not attempted to locate these very weakly bound complexes and will discuss only the transition states and product complexes. These two stationary points, together with additional analyses, reveal sufficient insight into the reaction energy profiles for our series of catalysts.

Using again the dispersion-corrected ZORA−BLYP−D3/TZ2P level of theory, we find a barrier of +29.5 kcal mol^{-1} for $Pd(PH_3)_2$, followed by a slightly lower barrier of +28.4 kcal mol^{-1} for $Pd(PMe_3)_2$. Thereafter, the barriers increase to +30.0 kcal mol^{-1} for oxidative addition to $Pd(PiPr_3)_2$ and +43.1 kcal mol^{-1} for $Pd(PtBu_3)_2$. For $Pd(PCy_3)_2$ and $Pd(PPh_3)_2$, we find that the barrier decreases monotonically in rather large steps to +31.1 and +20.9 kcal mol^{-1}, respectively (see Table 2). When solvation is accounted for (using toluene as solvent), these numbers are only slightly different (roughly 0.5 kcal mol^{-1}). A similar series of catalysts was studied by Liu and co-workers for the oxidative addition of arylhalides using dispersion-free DFT.[22] Interestingly, they found only a small decrease (2.3 kcal mol^{-1}) in barriers when going from $Pd(PiPr_3)_2$ to $Pd(PPh_3)_2$. Results obtained by Maseras et al. with dispersion-corrected DFT show that the barrier for CH_3Br

DOI: 10.1021/acscatal.5b01354
ACS Catal. 2015, 5, 5766−5775

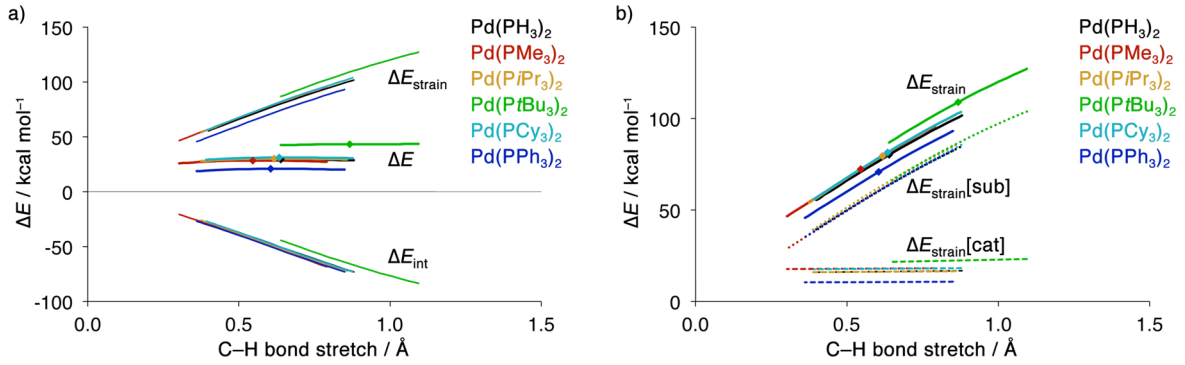

Figure 4. Activation strain analyses (a) and strain energy decomposition (b) along the reaction coordinate in the region around the TS for oxidative addition of CH_4 to $Pd(PR_3)_2$, computed at ZORA–BLYP–D3/TZ2P.

addition to $Pd(PPh_3)_2$ is ~4 kcal mol^{-1} lower than the barrier for addition to $Pd(PH_3)_2$.[23] Harvey and co-workers reported[24b] that the reaction barrier for arylhalide addition to $Pd(PPh_3)_2$ is ~1 kcal mol^{-1} higher than for $Pd(PCy_3)_2$ and that the barrier for the small $Pd(PH_3)_2$ is similar (for C–Cl activation) or slightly lower (for C–Br activation) than for the larger complexes.

The product complexes (PCs) reveal a trend similar to the transition states (TSs), as shown by a comparison of Tables 2 and 3. With the exception of $Pd(PMe_3)_2$ and $Pd(PtBu_3)_2$, all product complexes are roughly 5 kcal mol^{-1} lower in energy than the transition states and have slightly more bent P–Pd–P angles. For $Pd(PMe_3)_2$, the difference in energy is 9.4 kcal mol^{-1}. For $Pd(PtBu_3)_2$, we find a stable product complex (no imaginary frequencies) with a methane C–H stretch that is 0.16 Å greater than in the transition state geometry. However, the energy difference between the two is essentially zero (~0.01 kcal mol^{-1}), within the precision of our numerical techniques. In other words, the reaction leads to a product plateau for $Pd(PtBu_3)_2$, and the reverse reaction, that is, reductive elimination, proceeds without a barrier. We find that solvation by toluene induces a slightly larger effect on the reaction energies (the energy of PC relative to R) than was found for the barriers (the energy of TS relative to R), but the solvent effect on PC is still small, around 1 kcal mol^{-1}, and does not alter the trend.

Activation Strain Analyses. To reveal the origin of the differences in oxidative addition barrier height along our series of model catalysts, we have performed activation strain analyses along the approximated partial reaction energy profiles in the transition state region, obtained by the TV-IRC method[51] (Figure 4a). The harmonic approximation on which the TV-IRC method is based appears to be entirely valid only for $Pd(PH_3)_2$. For the other catalyst complexes, this approximation results in energy profiles in the TS region with energy maxima that are slightly higher in energy and shifted along the reaction coordinate as compared with the actual TS. In Figure 4, the positions of the actual transition states, that is, the fully optimized TS geometries, are indicated. It should be noted that the deviations of the TV-IRC maxima from the real transition states are small compared with the size of the effect we are seeking to explain, which is the overall increase in barrier height from $Pd(PH_3)_2$ to $Pd(PtBu_3)_2$, and the significant drop in barrier height along $Pd(PtBu_3)_2$, $Pd(PCy_3)_2$, and $Pd(PPh_3)_2$.

First, we note that the energy profiles and activation strain analyses for $Pd(PH_3)_2$, $Pd(PMe_3)_2$, and $Pd(PiPr_3)_2$ are rather similar. Not only do the energy profiles lie within a few kilocalories per mole, but also the components ΔE_{strain} and ΔE_{int} show only subtle variations (Figure 4a). Apparently, there are only minor differences in bite-angle flexibility (see also values for $\Delta E^{\ddagger}_{strain}$(cat) in Table 2) and catalyst–substrate bonding capability among these three catalysts. We will not focus on these subtleties, but instead look at the significant increase in barrier height when going to $Pd(PtBu_3)_2$. For the latter, we find a much larger increase in barrier, caused by a more destabilizing strain term as well as less stabilizing catalyst–substrate interaction, ΔE_{int} (see Figure 4a). Both these differences are directly related to the increased steric crowding associated with the isotropically bulky *t*Bu substituents. Decomposing the strain term into contributions from catalyst and substrate deformation (eq 1) reveals that the increase stems primarily from catalyst deformation (see Figure 4b). The curves for ΔE_{strain}(sub) roughly coincide for all catalysts, whereas the ΔE_{strain}(cat) term is clearly higher for $Pd(PtBu_3)_2$. This can be attributed to the decreased bite-angle flexibility of the catalyst, which requires more energy to bend (see also Figure 3), even though the ligand–metal–ligand angle of 130.8° at the TS is more linear than for any other catalyst in this series. At the same time, the bulkier tBu_3 substituents on the phosphine ligands lead to more Pauli repulsive interactions with the substrate, thereby weakening the interaction ΔE_{int} significantly. Note that the values in Table 2 are not suitable for such an analysis because they refer to the quite different positions at which the various TSs occur along the reaction coordinate (see C–H distances of activated bond in TS), a condition that prevents a consistent comparison.[56c]

Continuing along the series of catalyst complexes, we find that, upon going from $Pd(PtBu_3)_2$ to $Pd(PCy_3)_2$, the transition state is stabilized again. This is because both factors causing the high reaction barrier for $Pd(PtBu_3)_2$ disappear in the case of $Pd(PCy_3)_2$, which is nonlinear and has a high bite-angle flexibility. First, there is a lower strain energy, which, as shown in Figure 4b, is the result of a smaller contribution from ΔE_{strain}(cat). Thus, there is less deformation energy from bending the catalyst, although the catalyst's bite angle in the TS geometry is smaller than that of $Pd(PtBu_3)_2$ (see Table 2). Again, this is in line with the results shown in Figure 3, and a direct consequence of the steric attraction between the ligands. Second, when the ligands are bent farther away from the substrate, there is, compared to $Pd(PtBu_3)_2$, a relief in Pauli repulsion between catalyst and substrate. This strengthens the interaction energy, ΔE_{int}, for $Pd(PCy_3)_2$ compared with that of $Pd(PtBu_3)_2$. Going to $Pd(PPh_3)_2$, we find that, although the ligand–metal–ligand is even smaller than for $Pd(PCy_3)_2$, again,

DOI: 10.1021/acscatal.5b01354
ACS Catal. 2015, 5, 5766–5775

the catalyst deformation energy is lowered (Figure 4b) because of the increased steric attraction and resulting bite-angle flexibility. Because the interaction energy is not much different from that of $Pd(PCy_3)_2$ (Figure 4a), it is the lower strain term that directly causes the lowering of the reaction barrier. Note that we find that the interaction energy term for $Pd(PPh_3)_2$ is only slightly more stabilizing, even though the PPh_3 ligand is known to be a stronger electron donor than, for example, the PH_3 ligand. From Figure 4a, it is clear that any electronic effect stemming from this increased electron-donating capability is small compared with the effect on the ΔE_{strain} curves that results from the bite-angle flexibility. Interestingly, the barrier for $Pd(PPh_3)_2$ ends up as the lowest among this series of catalysts, 8.6 kcal mol^{-1} lower than the barrier for addition to the simple, archetypal $Pd(PH_3)_2$.

It follows that applying dispersion corrections can have significant effects on reaction barriers. This is neither because the additional *inter*molecular dispersion strengthens the catalyst−substrate interaction, which is strongest for $Pd(PtBu_3)_2$ and only around 9 kcal mol^{-1}, nor because of stronger donor−acceptor interactions between the catalyst and substrate that would result from destabilized d-hybrid orbitals upon increased bite-angle bending. These two effects would strengthen the catalyst-substrate interaction energy, ΔE_{int}. Rather, it is the difference in the strain energy, ΔE_{strain}, resulting from the variation among catalyst contributions, that causes the observed trends in reaction barriers.

Thus, the bite-angle flexibility of the catalyst, which is significantly increased by *intra*molecular dispersion interactions, leads to less destabilized reactants and therefore lower reaction energy profiles. This steric attraction effect is reminiscent of the bite-angle effect as described for palladium complexes with chelating ligands[4] and small, nonchelating ML_2 complexes.[10,11] Dispersion interactions play no important role for these small model complexes, for which the bite-angle flexibility or nonlinearity results entirely from electronic effects. For heavier halogen-substituted bisphosphine palladium complexes $Pd(PX_3)_2$, the contribution from dispersion was found to play a moderate role.[12] The catalyst complexes in the present study reveal that steric attraction as a result of dispersion interactions is of paramount importance to obtain quantitatively and even qualitatively accurate results for realistic catalyst complexes.

CONCLUSIONS

More bulky ligands in d^{10}-ML_2 complexes may *enhance*, instead of counteract, L−M−L bite-angle bending. Traditional behavior is found for $Pd(PH_3)_2$, $Pd(PMe_3)_2$, and $Pd(PtBu_3)_2$ complexes that have the expected linear L−M−L angle. Unexpectedly, however, $Pd(PiPr_3)_2$, $Pd(PCy_3)_2$, and $Pd(PPh_3)_2$ are bent. The more flexible or even nonlinear geometry translates into lower barriers for oxidative addition of bonds to these complexes. This follows from our quantum chemical analyses of the bonding in, and reactivity of, bisphosphine palladium complexes $Pd(PR_3)_2$ with varying steric bulk, based on relativistic dispersion-corrected DFT computations in combination with the activation strain model and quantitative MO theory.

Our analyses explain this dichotomy as they reveal that steric bulk may operate in two distinct ways: one is the usual steric repulsion deriving from overlap between closed-shell orbitals of intimate and isotropically bulky ligands; the second is steric attraction, which occurs between large but more planar ligands. Such ligands can build up relatively strong dispersion interactions between their large surfaces when they bend toward each other. The resulting stabilization favors bending and thus enhances nonlinearity or bite-angle flexibility. Thus, by introducing sizable ligands with anisotropically distributed bulk, one can enhance the bite-angle flexibility of a catalyst via a steric mechanism, on top of the electronic mechanisms that have been described previously.[10,12] This situation leads to relatively little catalyst activation strain and, thus, low reaction barriers for methane C−H activation by the rather congested $Pd(PCy_3)_2$ and $Pd(PPh_3)_2$ model catalysts. Interestingly, the lowest barrier among our series of model catalysts appears for the quite sizable $Pd(PPh_3)_2$ catalyst. Its C−H activation barrier of +20.9 kcal mol^{-1} is substantially below that of +29.5 kcal mol^{-1} that we find for the smallest catalyst complex, $Pd(PH_3)_2$. These results confirm the steric nature of the bite-angle effect on oxidative addition barriers and highlight the importance of the concept of bite-angle flexibility to describe catalyst activity.

Our findings not only demonstrate the importance of dispersion interactions in realistic catalyst complexes but also reveal how the concept of steric attraction can serve as a mechanism for tuning bite-angle flexibility and thereby activity of catalyst complexes.

ASSOCIATED CONTENT

Supporting Information

The Supporting Information is available free of charge on the ACS Publications website at DOI: 10.1021/acscatal.5b01354.

Cartesian coordinates and ADF total energies of all stationary points occurring in this study (PDF)

AUTHOR INFORMATION

Corresponding Author

*E-mail: F.M.Bickelhaupt@vu.nl.

Notes

The authors declare no competing financial interest.

ACKNOWLEDGMENTS

We thank the National Research School Combination − Catalysis (NRSC-C) and The Netherlands Organization for Scientific Research (NWO−CW and NWO-EW) for financial support.

REFERENCES

(1) (a) Diederich, F.; Stang, P. J. *Metal-Catalyzed Cross-Coupling Reactions*; Wiley-VCH: Weinheim, 1998. (b) Hartwig, J. F. *Organotransition Metal Chemistry: From Bonding to Catalysis*, 1st ed., University Science Books: Sausalito, 2010. (c) Luh, T.-Y.; Leung, M.-K.; Wong, K.-T. *Chem. Rev.* **2000**, *100*, 3187−3204. (d) Heck, R. F.; Nolley, J. P., Jr *J. Org. Chem.* **1972**, *37*, 2320−3222. (e) Stille, J. K. *Angew. Chem., Int. Ed. Engl.* **1986**, *25*, 508−523. (f) Miyaura, N.; Suzuki, A. *Chem. Rev.* **1995**, *95*, 2457−2483. (g) Littke, A. F.; Fu, G. C. *Angew. Chem., Int. Ed.* **2002**, *41*, 4176−4211.

(2) (a) Van Leeuwen, P. W. N. M.; Kamer, P. C. J.; Reek, J. N. H.; Dierkes, P. *Chem. Rev.* **2000**, *100*, 2741−2769. (b) Birkholz (née Gensow), M.-N.; Freixa, Z.; Van Leeuwen, P. W. N. M. *Chem. Soc. Rev.* **2009**, *38*, 1099−1118. (c) Otsuka, S. *J. Organomet. Chem.* **1980**, *200*, 191−205. (d) Low, J. J.; Goddard, W. A. *J. Am. Chem. Soc.* **1984**, *106*, 6928−6937. (e) Dierkes, P.; Van Leeuwen, P. W. N. M. *J. Chem. Soc., Dalton Trans.* **1999**, 1519−1529. (f) Freixa, Z.; Van Leeuwen, P. W. N. M. *Dalton Trans.* **2003**, 1890−1901. (g) Fazaeli, R.; Ariafard, A.; Jamshidi, S.; Tabatabaie, E. S.; Pishro, K. A. *J. Organomet. Chem.* **2007**, *692*, 3984−3993. (h) Su, M. D.; Chu, S. Y. *Inorg. Chem.* **1998**, *37*, 3400−3406. (i) Kozuch, S.; Amatore, C.; Jutand, A.; Shaik, S.

DOI: 10.1021/acscatal.5b01354
ACS Catal. 2015, 5, 5766−5775

Organometallics **2005**, *24*, 2319−2330. (j) Xue, L.; Lin, Z. *Chem. Soc. Rev.* **2010**, *39*, 1692−1705.
(3) Van Leeuwen, P. W. N. M. *Homogeneous Catalysis: Understanding the Art*; Kluwer Academic Publishers: Dordrecht, 2004.
(4) (a) Van Zeist, W.-J.; Visser, R.; Bickelhaupt, F. M. *Chem. - Eur. J.* **2009**, *15*, 6112−6115. (b) Van Zeist, W.-J.; Bickelhaupt, F. M. *Dalton Trans.* **2011**, *40*, 3028−3038.
(5) (a) Hofmann, P.; Heiss, H.; Müller, G. *Z. Naturforsch., B: J. Chem. Sci.* **1987**, *42*, 395−409. (b) Sakaki, S.; Biswas, B.; Sugimoto, M. *J. Chem. Soc., Dalton Trans.* **1997**, 803−809. (c) Zuidema, E.; Van Leeuwen, P. W. N. M.; Bo, C. *Organometallics* **2005**, *24*, 3703−3710.
(6) Albright, T. A.; Burdett, J. K.; Whangbo, M. H. *Orbital Interactions in Chemistry*, 2nd ed.; John Wiley & Sons: Hoboken, NJ, 2013.
(7) Carvajal, M. A.; Novoa, J. J.; Alvarez, S. *J. Am. Chem. Soc.* **2004**, *126*, 1465−1477.
(8) King, R. B. *Coord. Chem. Rev.* **2000**, *197*, 141−168.
(9) Ziegler, T. *Inorg. Chem.* **1985**, *24*, 1547−1552.
(10) Wolters, L. P.; Bickelhaupt, F. M. *ChemistryOpen* **2013**, *2*, 106−114.
(11) Wolters, L. P.; Van Zeist, W.-J.; Bickelhaupt, F. M. *Chem. - Eur. J.* **2014**, *20*, 11370−11381.
(12) Wolters, L. P.; Bickelhaupt, F. M. d^{10}-ML_2 Complexes: Structure, Bonding and Reactivity. In: *Structure and Bonding (Berlin)*; Eisenstein, O., Macgregor, S., Eds.; Springer: Berlin, 2015.
(13) (a) Socol, S. M.; Verkade, J. G. *Inorg. Chem.* **1984**, *23*, 3487−3439. (b) Rahman, M. M.; Liu, H. Y.; Prock, A.; Giering, W. P. *Organometallics* **1987**, *6*, 650−658. (c) Brown, T. L. *Inorg. Chem.* **1992**, *31*, 1286−1294. (d) Wilson, M. R.; Woska, D. C.; Prock, A.; Giering, W. P. *Organometallics* **1993**, *12*, 1742−1752. (e) Woo, T. K.; Ziegler, T. *Inorg. Chem.* **1994**, *33*, 1857−1863. (f) Woska, D.; Prock, A.; Giering, W. P. *Organometallics* **2000**, *19*, 4629−4638. (g) Suresh, C. *Inorg. Chem.* **2006**, *45*, 4982−4986.
(14) (a) Hamann, B. C.; Hartwig, J. F. *J. Am. Chem. Soc.* **1998**, *120*, 3694−3703. (b) Van Strijdonck, G. P. F.; Boele, M. D. K.; Kamer, P. C. J.; De Vries, J. G.; Van Leeuwen, P. W. N. M. *Eur. J. Inorg. Chem.* **1999**, *1999*, 1073−1076. (c) Carbó, J. J.; Maseras, F.; Bo, C.; Van Leeuwen, P. W. N. M. *J. Am. Chem. Soc.* **2001**, *123*, 7630−7637. (d) Galardon, E.; Ramdeehul, S.; Brown, J. M.; Cowley, A.; Hii, K. K.; Jutand, A. *Angew. Chem., Int. Ed.* **2002**, *41*, 1760−1763. (e) Gonsalvi, L.; Gaunt, J. A.; Adams, H.; Castro, A.; Sunley, G. J.; Haynes, A. *Organometallics* **2003**, *22*, 1047−1054. (f) Mann, G.; Shelby, Q.; Roy, A. H.; Hartwig, J. F. *Organometallics* **2003**, *22*, 2775−2789. (g) Stambuli, J. P.; Incarvito, C. D.; Bühl, M.; Hartwig, J. F. *J. Am. Chem. Soc.* **2004**, *126*, 1184−1194. (h) Barrios-Landeros, F.; Hartwig, J. F. *J. Am. Chem. Soc.* **2005**, *127*, 6944−6945. (i) Moncho, S.; Ujaque, G.; Lledos, A.; Espinet, P. *Chem. - Eur. J.* **2008**, *14*, 8986−8994. (j) Ariafard, A.; Yates, B. F. *J. Am. Chem. Soc.* **2009**, *131*, 13981−13991. (k) Barrios-Landeros, F.; Carrow, B. P.; Hartwig, J. F. *J. Am. Chem. Soc.* **2009**, *131*, 8141−8154. (l) Kefalidis, C. E.; Baudoin, O.; Clot, E. *Dalton Trans.* **2010**, *39*, 10528−10535. (m) Kozuch, S.; Shaik, S. *J. Mol. Catal. A: Chem.* **2010**, *324*, 120−126. (n) Nilsson Lill, S. O.; Ryberg, P.; Rein, T.; Bennström, E.; Norrby, P.-O. *Chem. - Eur. J.* **2012**, *18*, 1640−1649. (o) Kurbangalieva, A.; Carmichael, D.; Hii, K. K.; Jutand, A.; Brown, J. M. *Chem. - Eur. J.* **2014**, *20*, 1116−1125.
(15) Tanaka, M. *Acta Crystallogr., Sect. C: Cryst. Struct. Commun.* **1992**, *C48*, 739−740.
(16) Otsuka, S.; Yoshida, T.; Matsumoto, M.; Nakatsu, K. *J. Am. Chem. Soc.* **1976**, *98*, 5850−5858.
(17) Immirzi, A.; Musco, A. *J. Chem. Soc., Chem. Commun.* **1974**, *10*, 400−401.
(18) Immirzi, A.; Musco, A.; Zambelli, P.; Carturan, G. *Inorg. Chim. Acta* **1975**, *13*, L13−L14.
(19) Dinjus, E.; Leitner, W. *Appl. Organomet. Chem.* **1995**, *9*, 43−50.
(20) Ahlquist, M.; Fristrup, P.; Tanner, D.; Norrby, P.-O. *Organometallics* **2006**, *25*, 2066−2073.
(21) Ananikov, V. P.; Musaev, D. G.; Morokuma, K. *Eur. J. Inorg. Chem.* **2007**, *2007*, 5390−5399.
(22) Li, Z.; Fu, Y.; Guo, Q.-X.; Liu, L. *Organometallics* **2008**, *27*, 4043−4049.
(23) Besora, M.; Gourlaouen, C.; Yates, B.; Maseras, F. *Dalton Trans.* **2011**, *40*, 11089−11094.
(24) (a) Jover, J.; Fey, N.; Purdie, M.; Lloyd-Jones, G. C.; Harvey, J. N. *J. Mol. Catal. A: Chem.* **2010**, *324*, 39−47. (b) McMullin, C. L.; Fey, N.; Harvey, J. N. *Dalton Trans.* **2014**, *43*, 13545−13556.
(25) Ahlquist, M. S. G.; Norrby, P.-O. *Angew. Chem., Int. Ed.* **2011**, *50*, 11794−11797.
(26) (a) Hoffmann, R.; Levin, C. C.; Moss, R. A. *J. Am. Chem. Soc.* **1973**, *95*, 629−631. (b) Sauers, R. R. *J. Chem. Educ.* **1996**, *73*, 114−116.
(27) Marzabadi, C. H.; Anderson, J. E.; Gonzalez-Outeirino, J.; Gaffney, P. R. J.; White, C. G. H.; Tocher, D. A.; Todaro, L. J. *J. Am. Chem. Soc.* **2003**, *125*, 15163−15173.
(28) Lin, C.-Y.; Guo, J.-D.; Fettinger, J. C.; Nagase, S.; Grandjean, F.; Long, G. J.; Chilton, N. F.; Power, P. P. *Inorg. Chem.* **2013**, *52*, 13584−13593.
(29) (a) Jacobsen, H.; Cavallo, L. *ChemPhysChem* **2012**, *13*, 562−569. (b) Grimme, S. *ChemPhysChem* **2012**, *13*, 1407−1409.
(30) Grimme, S.; Djukic, J. P. *Inorg. Chem.* **2011**, *50*, 2619−2628.
(31) Hansen, A.; Bannwarth, C.; Grimme, S.; Petrović, P.; Werlé, C.; Djukic, J.-P. *ChemistryOpen* **2014**, *3*, 177−189.
(32) Te Velde, G.; Bickelhaupt, F. M.; Baerends, E. J.; Fonseca Guerra, C.; Van Gisbergen, S. J. A.; Snijders, J. G.; Ziegler, T. *J. Comput. Chem.* **2001**, *22*, 931−967.
(33) Fonseca Guerra, C.; Snijders, J. G.; Te Velde, G.; Baerends, E. J. *Theor. Chem. Acc.* **1998**, *99*, 391−403.
(34) Baerends, E. J.; Ziegler, T.; Autschbach, J.; Bashford, D.; Bérces, A.; Bickelhaupt, F. M.; Bo, C.; Boerrigter, P. M.; Cavallo, L.; Chong, D. P.; Deng, L.; Dickson, R. M.; Ellis, D. E.; Van Faassen, M.; Fan, L.; Fischer, T. H.; Fonseca Guerra, C.; Ghysels, A.; Giammona, A.; Van Gisbergen, S. J. A.; Götz, A. W.; Groeneveld, J. A.; Gritsenko, O. V.; Grüning, M.; Gusarov, S.; Harris, F. E.; Van Den Hoek, P.; Jacob, C. R.; Jacobsen, H.; Jensen, L.; Kaminski, J. W.; Van Kessel, G.; Kootstra, F.; Kovalenko, A.; Krykunov, M. V.; Van Lenthe, E.; McCormack, D. A.; Michalak, A.; Mitoraj, M.; Neugebauer, J.; Nicu, V. P.; Noodleman, L.; Osinga, V. P.; Patchkovskii, S.; Philipsen, P. H. T.; Post, D.; Pye, C. C.; Ravenek, W.; Rodríguez, J. I.; Ros, P.; Schipper, P. R. T.; Schreckenbach, G.; Seldenthuis, J. S.; Seth, M.; Snijders, J. G.; Solà, M.; Swart, M.; Swerhone, D.; Te Velde, G.; Vernooijs, P.; Versluis, L.; Visscher, L.; Visser, O.; Wang, F.; Wesolowski, T. A.; Van Wezenbeek, E. M.; Wiesenekker, G.; Wolff, S. K.; Woo, T. K.; Yakovlev, A. L.. *ADF 2012 and ADF 2013, Scientific Computing & Modelling (SCM), Theoretical Chemistry*; Vrije Universiteit: Amsterdam, The Netherlands, http://www.scm.com/.
(35) (a) Swart, M.; Bickelhaupt, F. M. *Computer software (QUILD)*; Vrije Universiteit: Amsterdam, The Netherlands, 2006. (b) Swart, M.; Bickelhaupt, F. M. *Int. J. Quantum Chem.* **2006**, *106*, 2536−2544. (c) Swart, M.; Solà, M.; Bickelhaupt, F. M. *J. Comput. Chem.* **2007**, *28*, 1551−1560.
(36) (a) Boerrigter, P. M.; Te Velde, G.; Baerends, E. J. *Int. J. Quantum Chem.* **1988**, *33*, 87−113. (b) Te Velde, G.; Baerends, E. J. *J. Comput. Phys.* **1992**, *99*, 84−98.
(37) Franchini, M.; Philipsen, P. H. T.; Visscher, L. *J. Comput. Chem.* **2013**, *34*, 1819−1827.
(38) Van Lenthe, E.; Baerends, E. J. *J. Comput. Chem.* **2003**, *24*, 1142−1156.
(39) Versluis, L.; Ziegler, T. *J. Chem. Phys.* **1988**, *88*, 322−328.
(40) Slater, J. C. *Quantum Theory of Molecules and Solids*; McGraw-Hill: New York, 1974, Vol. *4*.
(41) (a) Becke, A. D. *J. Chem. Phys.* **1986**, *84*, 4524−4529. (b) Becke, A. D. *Phys. Rev. A: At., Mol., Opt. Phys.* **1988**, *38*, 3098−3100.
(42) (a) Lee, C.; Yang, W.; Parr, R. G. *Phys. Rev. B: Condens. Matter Mater. Phys.* **1988**, *37*, 785−789. (b) Johnson, B. G.; Gill, P. M. W.; Pople, J. A. *J. Chem. Phys.* **1993**, *98*, 5612−5626. (c) Russo, T. V.; Martin, R. L.; Hay, P. J. *J. Chem. Phys.* **1994**, *101*, 7729−7737.
(43) Grimme, S.; Antony, J.; Ehrlich, S.; Krieg, H. *J. Chem. Phys.* **2010**, *132*, 154104−154119.

DOI: 10.1021/acscatal.5b01354
ACS Catal. 2015, 5, 5766−5775

(44) (a) Van Lenthe, E.; Baerends, E. J.; Snijders, J. G. *J. Chem. Phys.* **1994**, *101*, 9783−9792. (b) Van Lenthe, E.; Van Leeuwen, R.; Baerends, E. J.; Snijders, J. G. *Int. J. Quantum Chem.* **1996**, *57*, 281−293. For a benchmark and performance studies involving the ZORA-BLYP/TZ2P approach, see: (c) De Jong, G. Th.; Solà, M.; Visscher, L.; Bickelhaupt, F. M. *J. Chem. Phys.* **2004**, *121*, 9982−9992. (d) De Jong, G. Th.; Geerke, D. P.; Diefenbach, A.; Bickelhaupt, F. M. *Chem. Phys.* **2005**, *313*, 261−270. (e) De Jong, G. Th.; Bickelhaupt, F. M. *J. Chem. Theory Comput.* **2006**, *2*, 322−335.
(45) (a) Klamt, A.; Schüürman, G. *J. Chem. Soc., Perkin Trans. 2* **1993**, 799−805. (b) Klamt, A. *J. Phys. Chem.* **1995**, *99*, 2224−2235.
(46) Pye, C. C.; Ziegler, T. *Theor. Chem. Acc.* **1999**, *101*, 396−408.
(47) Allinger, N. L.; Zhou, X.; Bergsma, J. *J. Mol. Struct.: THEOCHEM* **1994**, *312*, 69−83.
(48) Swart, M.; Rösler, E.; Bickelhaupt, F. M. *Eur. J. Inorg. Chem.* **2007**, *2007*, 3646−3654.
(49) Riley, K. E.; Vondrasek, J.; Hobza, P. *Phys. Chem. Chem. Phys.* **2007**, *9*, 5555−5560.
(50) (a) Bérces, A.; Dickson, R. M.; Fan, L.; Jacobsen, H.; Swerhone, D.; Ziegler, T. *Comput. Phys. Commun.* **1997**, *100*, 247−262. (b) Jacobsen, H.; Bérces, A.; Swerhone, D.; Ziegler, T. *Comput. Phys. Commun.* **1997**, *100*, 263−276. (c) Wolff, S. K. *Int. J. Quantum Chem.* **2005**, *104*, 645−659.
(51) Van Zeist, W. J.; Koers, A. H.; Wolters, L. P.; Bickelhaupt, F. M. *J. Chem. Theory Comput.* **2008**, *4*, 920−928.
(52) Fukui, K. *Acc. Chem. Res.* **1981**, *14*, 363−368.
(53) Deng, L.; Ziegler, T.; Fan, L. *J. Chem. Phys.* **1993**, *99*, 3823−3835.
(54) Van Zeist, W. J.; Fonseca Guerra, C.; Bickelhaupt, F. M. *J. Comput. Chem.* **2008**, *29*, 312−315.
(55) (a) Bickelhaupt, F. M.; Van Eikema Hommes, N. J. R.; Fonseca Guerra, C.; Baerends, E. J. *Organometallics* **1996**, *15*, 2923−2931. (b) Fonseca Guerra, C.; Handgraaf, J.-W.; Baerends, E. J.; Bickelhaupt, F. M. *J. Comput. Chem.* **2004**, *25*, 189−210.
(56) (a) De Jong, G. Th.; Bickelhaupt, F. M. *J. Chem. Theory Comput.* **2007**, *3*, 514−529. (b) Bickelhaupt, F. M. *J. Comput. Chem.* **1999**, *20*, 114−128. (c) De Jong, G. Th.; Bickelhaupt, F. M. *ChemPhysChem* **2007**, *8*, 1170−1181. (d) Van Zeist, W.-J.; Bickelhaupt, F. M. *Org. Biomol. Chem.* **2010**, *8*, 3118−327. (e) Fernandez, I.; Bickelhaupt, F. M. *Chem. Soc. Rev.* **2014**, *43*, 4953−4967. (f) Wolters, L. P.; Bickelhaupt, F. M. *WIREs Comput. Mol. Sci.* **2015**, *5*, 324−343.
(57) (a) Bickelhaupt, F. M.; Baerends, E. J. In *Reviews in Computational Chemistry*; Lipkowitz, K. B., Boyd, D. B., Eds.; Wiley-VCH: New York, 2000; Vol. *15*; pp 1−86. (b) Bickelhaupt, F. M.; Nibbering, N. M. M.; Van Wezenbeek, E. M.; Baerends, E. J. *J. Phys. Chem.* **1992**, *96*, 4864−4873. (c) Bickelhaupt, F. M.; Diefenbach, A.; De Visser, S. P.; De Koning, L. J.; Nibbering, N. M. M. *J. Phys. Chem. A* **1998**, *102*, 9549−9553. (d) Ziegler, T.; Rauk, A. *Inorg. Chem.* **1979**, *18*, 1755−1759.
(58) Tolman, C. A. *Chem. Rev.* **1977**, *77*, 313−348.
(59) Brown, T. L.; Lee, K. J. *Coord. Chem. Rev.* **1993**, *128*, 89−116.
(60) (a) Bilbrey, J. A.; Kazez, A. H.; Locklin, J.; Allen, W. D. *J. Comput. Chem.* **2013**, *34*, 1189−1197. (b) Bilbrey, J. A.; Kazez, A. H.; Locklin, J.; Allen, W. D. *J. Chem. Theory Comput.* **2013**, *9*, 5734−5744.
(61) Zhang, J.; Dolg, M. *Chem. - Eur. J.* **2014**, *20*, 13909−13912.
(62) Grimme, S.; Schreiner, P. R. *Angew. Chem., Int. Ed.* **2011**, *50*, 12639−12642.
(63) Grimme, S. *Angew. Chem., Int. Ed.* **2008**, *47*, 3430−3434.

DOI: 10.1021/acscatal.5b01354
ACS Catal. 2015, 5, 5766−5775